

A Robust Volumetric Transformer for Accurate 3D Tumor Segmentation

Himashi Peiris¹, Munawar Hayat³, Zhaolin Chen^{1,2}, Gary Egan², Mehrtash Harandi¹

¹ Department of Electrical and Computer Systems Engineering, Faculty of Engineering, Monash University, Melbourne, Australia.

² Monash Biomedical Imaging (MBI), Monash University, Melbourne, Australia.

³ Department of Data Science & AI, Faculty of IT, Monash University, Melbourne, Australia.

{Edirisinghe.Peiris, Munawar.Hayat, Zhaolin.Chen, Gary.Egan, Mehrtash.Harandi}@monash.edu

Abstract. We propose a Transformer architecture for volumetric segmentation, a challenging task that requires keeping a complex balance in encoding local and global spatial cues, and preserving information along all axes of the volume. Encoder of the proposed design benefits from self-attention mechanism to simultaneously encode local and global cues, while the decoder employs a parallel self and cross attention formulation to capture fine details for boundary refinement. Empirically, we show that the proposed design choices result in a computationally efficient model, with competitive and promising results on the Medical Segmentation Decathlon (MSD) brain tumor segmentation (BraTS) Task. We further show that the representations learned by our model are robust against data corruptions. [Our code implementation is publicly available.](#)

Keywords: Pure Volumetric Transformer · Tumor Segmentation

1 Introduction

Inspired by the strong empirical results of the transformer based models in computer vision [8,5,15], their promising generalization and robustness characteristics [21], and their flexibility to model long range interactions, we propose a volumetric transformer architecture for segmentation of 3D medical image modalities (*e.g.*, MRI, CT), called VT-UNet. Earlier efforts to develop transformer based segmentation models for 3D medical scans have been shown to outperform state-of-the-art CNN counterparts [4]. However, these methods divide 3D volumes into 2D slices and process 2D slices as inputs [4,6]. As such, considerable and potentially critical volumetric information, essential to encapsulating inter-slice dependencies, is lost. While some hybrid approaches (using both convolutional

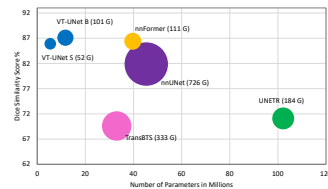


Fig. 1: The model size vs Dice Similarity Coefficient (DSC) is shown in this plot. Circle size indicates Computational Complexity by FLOPs. VT-UNet achieves highest DSC compared to SOTA methods while maintaining a smaller model size and low computational complexity.

blocks and Transformer layers) keep the 3D volumetric data intact [25,9,30], the design of purely transformer based architecture, capable of keeping intact the volumetric data at input, is yet unexplored in the literature. Our work takes the first step in this direction, and proposes a model, which not only achieves better segmentation performance, but also demonstrates better robustness against data artefacts. The Transformer models have highly dynamic and flexible receptive field and are able to capture long-range interactions, yet designing a Transformer based UNet architecture for volumetric segmentation remains a challenging task. This is because: **(1)** Encapsulating voxel information and capturing the connections between arbitrary positions in the volumetric sequence is not straightforward. Compared with Transformer based approaches for 2D image segmentation [4], the data in each slice of the volume is connected to three views and discarding either of them can be detrimental. **(2)** Preserving spatial information in a volume is a daunting task. Even for 2D images, while breaking the image into patches and projecting patches into tokens as introduced in Vision Transformer (ViT), local structural cues can be lost, as shown in Tokens-to-token ViT [28]. Effectively encoding the local cues while simultaneously capturing global interactions along multiple axes of a volume is therefore a challenging task. **(3)** Due to the quadratic complexity of the self-attention, and large size of 3D volume tensor inputs, designing a Transformer based segmentation model, which is computationally efficient, requires careful design considerations. Our proposed VT-UNet model effectively tackles the above design challenges by proposing a number of modules. In our UNet based architecture, we develop two types of Transformer blocks. First, our blocks in the encoder which directly work on the 3D volumes, in a hierarchical manner, to jointly capture the local and global information, similar in spirit to the Swin Transformer blocks [14]. Secondly, for the decoder, we introduce parallel cross-attention and self-attention in the expansive path, which creates a bridge between queries from the decoder and keys & values from the encoder. By this parallelization of the cross-attention and self-attention, we aim to preserve the full global context during the decoding process, which is important for the task of segmentation. Since VT-UNet is free from convolutions and combines attention outputs from two modules during the decoding, the order of the sequence is important to get accurate predictions. Inspired by [24], apart from applying relative positional encoding while computing attention in each Transformer block, we augment the decoding process and inject the complementary information extracted from Fourier feature positions of the tokens in the sequence. In summary, our major contributions are, **(1)** We reformulate volumetric tumor segmentation from a sequence-to-sequence perspective, and propose a UNet shaped *Volumetric Transformer* for multi-modal medical image segmentation. **(2)** We design an encoder block with two consecutive self attention layers to jointly capture local and global contextual cues. Further, we design a decoder block which enables parallel (shifted) window based self and cross attention. This parallelization uses one shared projection of the *queries* and independently computes cross and self attention. To further enhance our features in the decoding, we propose a convex combination approach along with

Fourier positional encoding. **(3)** Incorporating our proposed design choices, we substantially limit the model parameters while maintaining lower FLOPs compared to existing approaches (see Fig. 1). **(4)** We conduct extensive evaluations and show that our design achieves state-of-the-art volumetric segmentation results, alongwith enhanced robustness to data artefacts.

2 Methodology

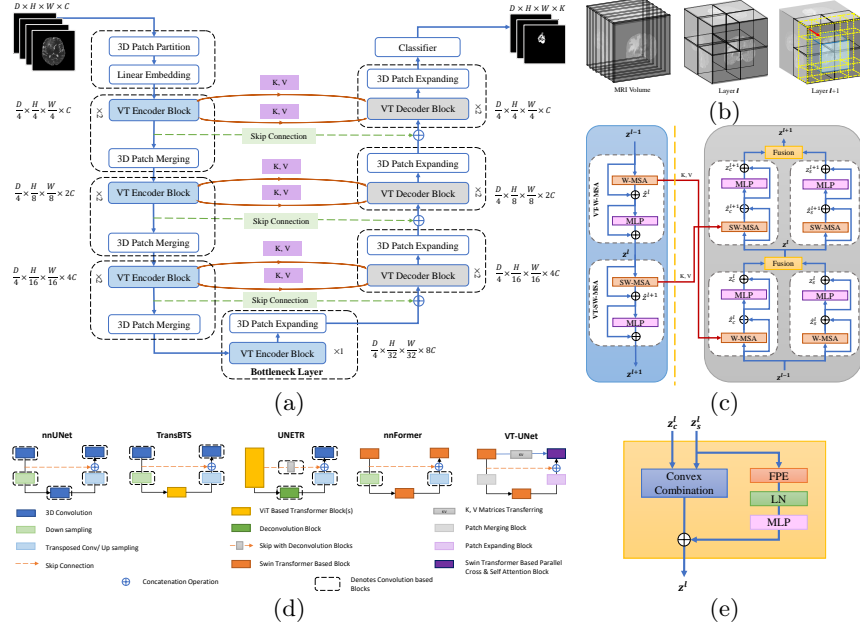


Fig. 2: (a) Illustrates VT-UNet Architecture. Here, k denotes the number of classes. (b) shows visualization of Volumetric Shifted Windows. Consider an MRI volume of size $D \times H \times W$ with $D = H = W = 8$ for the sake of illustration. Further, let the window size for partitioning the volume be $P \times M \times M$ with $P = M = 4$. Here, layer l adopts the regular window partition in the first step of Volumetric Transformer(VT) block which results in $2 \times 2 \times 2 = 8$ windows. Inside layer $l + 1$, volumetric windows are shifted by $(\frac{P}{2}, \frac{M}{2}, \frac{M}{2}) = (2, 2, 2)$ tokens. This results in $3 \times 3 \times 3 = 27$ windows. (c) shows VT Encoder-Decoder Structure. (d)Encoder-Decoder structural comparison with other SOTA methods. The proposed VT-UNet architecture has no convolution modules and is purely based on Transformer blocks. (e) Illustrates the structure of the Fusion Module.

We denote vectors and matrices in bold lower-case \mathbf{x} and bold upper-case \mathbf{X} , respectively. Let $\mathbf{X} = \{\mathbf{x}_1, \mathbf{x}_2, \dots, \mathbf{x}_\tau\}$, $\mathbf{x}_i \in \mathbb{R}^C$ be a sequence representing a signal of interest (*e.g.*, an MRI volume). We call each \mathbf{x}_i a token. We assume that tokens, in their original form, might not be optimal for defining the span. Therefore, in Self-Attention (SA), we define the span by learning a linear mapping from the input tokens. This we can show with $\mathbb{R}^{\tau \times C_v} \ni \mathbf{V} = \mathbf{XW}_V$, where we stack tokens \mathbf{x}_i s into the rows of \mathbf{X} (*i.e.*, $\mathbf{X} = [\mathbf{x}_1 | \mathbf{x}_2 | \dots | \mathbf{x}_\tau]^\top$). Following previous work by Hu *et al.* [10], we use a slight modification of the self-attention [24](see [13]) in our task as follows:

$$\text{SA}(\mathbf{Q}, \mathbf{K}, \mathbf{V}) = \text{SoftMax}\left(\frac{\mathbf{QK}^\top}{\sqrt{C}} + \mathbf{B}\right)\mathbf{V}, \quad (1)$$

where $\mathbb{R}^{\tau \times \tau} \ni \mathbf{B}$ is trainable and acts as a relative positional bias across tokens in the volume with $\mathbf{V} = \mathbf{XW}_V$, $\mathbf{K} = \mathbf{XW}_K$, and $\mathbf{Q} = \mathbf{XW}_Q$. In practice, computing SA for multiple attention heads several times in parallel is called Multi-head Self-Attention (MSA). Eq. (1) is the basic building block of our Volumetric Transformer Window based Multi-head Self-Attention (VT-W-MSA), and the Volumetric Transformer Shifted Window based Multi-head Self-Attention (VT-SW-MSA), discussed next.

Overview of VT-UNet. Fig. 2 shows the conceptual diagram of the proposed volumetric transformer network or **VT-UNet** for short. The input to our model is a 3D volume of size $D \times H \times W \times C$. The output is a $D \times H \times W \times K$ dimensional volume, representing the presence/absence of voxel-level class labels (K is the number of classes). Below, we discuss architectural form of the VT-UNet modules and explain the functionality and rationals behind our design in detail.

The VT Encoder. The VT encoder consists of 3D Patch Partitioning layer together with Linear Embedding layer, and 3D Patch merging layer followed by two successive VT encoder blocks.

3D Patch Partitioning. Transformer-based models work with a sequence of tokens. The very first block of VT-UNet accepts a $D \times H \times W \times C$ dimensional medical volume (*e.g.*, MRI) and creates a set of tokens by splitting the 3D volume into non-overlapping 3D patches (see Fig. 2 (b)). The size of partitioning kernel is $P \times M \times M$, resulting in describing the volume by $\tau = \lfloor D/P \rfloor \times \lfloor H/M \rfloor \times \lfloor W/M \rfloor$ tokens. The 3D patch partitioning is followed by a linear embedding to map each token with dimensionality $P \times M \times M$ to a C dimensional vector. Typical values for M , P and C according to our experiments are 4, 4, and 72, respectively.

VT Encoder Block. In ViT, tokens carry significant spatial information due to the way they are constructed. The importance of performing SA by windowing in ViT has been shown in several recent studies, most notably in Swin Transformer [14]. Following a similar principal in the design of Swin Transformers, albeit for volumetric data, we propose 3D windowing operations in our VT Encoder Blocks (**VT-Enc-Blks**). In particular, we propose two types of windowing, namely regular window and shifted window, which we show by **VT-W-MSA** and **VT-SW-MSA** for simplicity, respectively. Fig. 2b provides the design specifics of **VT-W-MSA** and **VT-SW-MSA**, while Fig. 2 (b) illustrates the windowing operation. Both VT-W-MSA and VT-SW-MSA employ attention layers with windowing, followed by a 2-layer Multi Layer Perceptron (MLP) with Gaussian Error Linear Unit (GELU) non-linearity in between. A Layer Normalization (LN) is applied before every MSA and MLP, and a residual connection is applied after each module. The windowing enables us to inject inductive bias in modeling long range dependencies between tokens. In both VT-W-MSA and VT-SW-MSA, attention across tokens within a window helps representation learning. In the VT-W-MSA, we split the volume evenly into smaller non-overlapping windows as illustrated in Fig. 2 (b). Since tokens in adjacent windows cannot see each other with VT-W-MSA, we make use of a shifted window in VT-SW-MSA (see the right most panel Fig. 2 (b)) which bridges tokens in adjacent windows of VT-W-MSA. The windowing is inspired

by the Swin Transformer [14] and can be understood as generalization to volumetric data. Note that the windowing operation in our work resembles [15] that extends the benefits of windowing beyond images to videos. Putting everything together, the VT-Enc-Blk realizes the following functionality:

$$\begin{aligned} \hat{\mathbf{z}}^l &= \text{VT-W-MSA}(\text{LN}(\mathbf{z}^{l-1})) + \mathbf{z}^{l-1}, & \hat{\mathbf{z}}^{l+1} &= \text{VT-SW-MSA}(\text{LN}(\mathbf{z}^l)) + \mathbf{z}^l, \\ \mathbf{z}^l &= \text{MLP}(\text{LN}(\hat{\mathbf{z}}^l)) + \hat{\mathbf{z}}^l, & \mathbf{z}^{l+1} &= \text{MLP}(\text{LN}(\hat{\mathbf{z}}^{l+1})) + \hat{\mathbf{z}}^{l+1}, \end{aligned} \quad (2)$$

where $\hat{\mathbf{z}}^l$ and \mathbf{z}^l denote the output features of the VT-W-MSA module and the MLP module for block l , respectively.

3D Patch Merging. We make use of 3D patch merging blocks to generate feature hierarchies in the encoder of VT-UNet. Having such hierarchies is essential to generate finer details in the output for the dense prediction tasks [14,7].

After every VT-Enc-Blk, we merge adjacent tokens along the spatial axes in a non-overlapping manner to produce new tokens. In doing so, we first concatenate features of each group of 2×2 neighboring tokens. The resulting vector is projected via a linear mapping to a space where the channel dimensionality of the tokens is doubled (see Fig. 2). The benefit of patch merging is not limited to feature hierarchies. The computational complexity of SA is quadratic in the number of tokens [14,15]. As such, patch merging reduces the FLOPs count of the VT-UNet by a factor of 16 after each VT-Enc-Blk. To give the reader a better idea and as we will discuss in §Sec. 4, the tiny VT-UNet model uses only 6.7% FLOPs in comparison to its fully volumetric CNN counterpart [16] while achieving a similar performance (slightly better indeed)! Please note that the patch merging block is not used in the bottleneck stage.

The VT Decoder. After bottleneck layer which consists of a VT-Enc-Blk together with 3D Patch Expanding layer, the VT decoder starts with successive VT Decoder Blocks (**VT-Dec-Blks**), 3D patch expanding layers and a classifier at the end to produce the final predictions. There are some fundamental design differences between VT-Enc-Blk and VT-Dec-Blk which we will discuss next.

3D Patch Expanding. This functionality is used to somehow revert the effect of patch merging. In other words and in order to construct the output with the same spatial-resolution as the input, we need to create new tokens in the decoder. For the sake of discussion, consider the patch expanding after the bottleneck layer (see the middle part of Fig. 2). The input tokens to the patch expanding are of dimensionality $8C$. In the patch expanding, we first increase the dimensionality of the input tokens by a factor of two using a linear mapping. Following a reshaping, we can obtain 2×2 tokens with dimensionality $4C$ from the resulting vector of dimensionality $2 \times 8C$. This, we will reshape along the spatial axes and hence for $D/4 \times H/32 \times W/32 \times 8C$, we create $D/4 \times H/16 \times W/16 \times 4C$ tokens.

VT Decoder Block. The UNet [20] and its variants [18,31] make use of lateral connections between the encoder and the decoder to produce fine-detailed predictions. This is because the spatial information is lost, at the expense of attaining higher levels of semantics, as the input passes through the encoder. The lateral connections in the UNet makes it possible to have the best of both

worlds, spatial information from lower layers and semantic information from upper layers (along the computational graph). Having this in mind, we propose a hybrid form of SA at the decoder side (see Fig. 2b for an illustration). Each VT-Dec-Blk receives the generated tokens of its previous VT-Dec-Blk along with the key (\mathbf{K}_E) and value (\mathbf{V}_E) tokens from the VT-Enc-Blk sitting at the same stage of VT-UNet, see Fig. 2a. Recall that a VT-Enc-Blk has two SA blocks with regular and shifted windowing operations. VT-Dec-Blk enjoys similar windowing operations but makes use of four SA blocks grouped into SA module and Cross Attention(CA) module. The functionality can be described as:

$$\text{SA}_r = \text{SA}(\mathbf{Q}_D, \mathbf{K}_D, \mathbf{V}_D), \quad \text{CA}_l = \text{SA}(\mathbf{Q}_D, \mathbf{K}_E, \mathbf{V}_E). \quad (3)$$

Here, r and l , denote right and left branches of the decoder module. The right branch of the SA acts on tokens generated by the previous VT-Dec-Blk according to Eq. (3). We emphasize on the flow of information from the decoder by the subscript D therein. The left branch of the CA, however, uses the queries generated by the decoder along with the keys and values obtained from the VT-Enc-Blk at the same level in the computation graph. The idea here is to use the basis spanned by the encoder (which is identified by values) along with keys to benefit from spatial information harvested by the encoder. These blocks, also use the regular and shifted windowing to inject more inductive bias into the model. Note that the values and keys from the SA with the same windowing operation should be combined, hence the criss-cross connection form in Fig. 2 (c).

Remark 1. One may ask why values and keys are considered from the encoder. We indeed studied other possibilities such as employing queries and keys from the encoder while generating values by the decoder. Empirically, the form described in Eq. (3) is observed to deliver better and more robust outcomes and hence our choice in VT-UNet⁴.

Fusion Module. As illustrated in Fig. 2 (e), tokens generated from the CA module and MSA module are combined together and fed to the next VT-Dec-Blk, \mathbf{z}^l is calculated using by a linear function as:

$$\mathbf{z}^l = \alpha \hat{\mathbf{z}}_c^l + (1 - \alpha) \hat{\mathbf{z}}_s^l + \mathcal{F}(\hat{\mathbf{z}}_s^l), \quad (4)$$

where $\mathcal{F}(\cdot)$ denotes Fourier Feature Positional Encoding (FPE) and α controls the contribution from each CA and MSA module. Aiming for simplicity, in fusing tokens generated by the CA and MSA, we use a linear combination with $\alpha = 0.5$ ⁵.

Classifier Layer. After the final 3D patch expanding layer in the decoder, we introduce a classifier layer which includes a 3D convolutional layer to map deep C dimensional features to K segmentation classes.

⁴ We empirically observed that employing keys and values from the encoder in CA yields faster convergence of VT-UNet. This, we conjecture, is due to having extra connections from the decoder to encoder during the back-propagation which might facilitate gradient flow.

⁵ Breaking the Symmetry: This results in a symmetry, meaning that swapping $\hat{\mathbf{z}}_c^l$ and $\hat{\mathbf{z}}_s^l$ does not change the output. To break this symmetry and also better encapsulate object-aware representations that are critical for anatomical pixel-wise segmentation, we supplement the tokens generated from MSA by the 3D FPE. The 3D FPE employs sine and cosine functions with different frequencies [24] to yield a unique encoding scheme for each token. The main idea is to use a sine/cosine function with a high frequency and modulate it across the dimensionality of the tokens while changing the frequency according to the location of the token within the 3D volume.

A note on computational complexity. The computational complexity of the SA described in Eq. (1) is dictated by computations required for obtaining $\mathbf{Q}, \mathbf{K}, \mathbf{V}$, computing \mathbf{QK}^\top and obtaining the resulting tokens by applying the output of the Softmax (which is a $\tau \times \tau$ matrix) to \mathbf{V} . This adds up to $\mathcal{O}(3\tau C^2 + 2\tau^2 C)$, where C and τ are the dimensionality and the number of tokens, respectively. Windowing will reduce the computational load of the SA according to $\mathcal{O}(3\tau C^2 + 2\tau\kappa C)$ where we have assumed that tokens are grouped into κ windows and SA is applied within each window. In our problem, where tokens are generated from volumetric data, $\tau \gg \kappa$ and hence windowing not only helps in having better discriminatory power, but also it helps in reducing the computational load⁶.

3 Related Work

Vision Transformers have shown superior empirical results for different computer vision tasks [23,2,15], with promising characteristics. For example and as compared with the CNNs, they are less biased towards texture [17], and show better generalization and robustness [21,17]. Transformers have also been recently investigated for image segmentation [29,6,4]. TransUNet [6] is the first Transformer based approach for medical image segmentation. It adapts a UNet structure, and replaces the bottleneck layer with ViT [8] where patch embedding is applied on a feature map generated from CNN encoder (where input is a 2D slice of 3D volume). Unlike these hybrid approaches (using both convolutions and self-attention), Cao *et al.* [4] proposed Swin-UNet, a purely transformer based network for medical image segmentation. It inherits swin-transformer blocks [14] and shows better segmentation results over TransUNet [6]. The 3D version of TransUNet [6], called TransBTS [25] has a CNN encoder-decoder design and a Transformer as the bottleneck layer. Zhou *et al.* [30] proposed nnFormer with 3D Swin Transformer based blocks as encoder and decoder with interleaved stem of convolutions. A model which employs a transformer as the encoder and directly connects intermediate encoder outputs to the the decoder via skip connections is proposed in [9]. The encoder-decoder structural comparison of SOTA methods are shown in Fig. 2 (d). The aforementioned transformer based approaches for 3D medical image segmentation have shown their promises, by achieving better performances compared with their CNN counterparts. Our proposed model, on the other hand, processes the volumetric data in its entirety, thus fully encoding the interactions between slices. Moreover, our proposed model is built purely based on Transformers and introduces lateral connections to perform CA along-with SA in the encoder-decoder design. These design elements contributed in achieving better segmentation performance, along-with enhanced robustness.

⁶ For the sake of simplicity and explaining the key message, we have made several assumptions in our derivation. First, we have assumed $C_k = C_v = C$. We also did not include the FLOPs needed to compute the softmax. Also, in practice, one uses a multi-head SA, where the computation is break down across several parallel head working on lower dimensional spaces (*e.g.*, on for \mathbf{V} , we use C/h dimensional spaces where h is the number of heads). This will reduce the computational load accordingly. That said, the general conclusion provided here is valid.

4 Experiments

Method	Average		WT		ET		TC	
	HD95 ↓	DSC ↑	HD95 ↓	DSC ↑	HD95 ↓	DSC ↑	HD95 ↓	DSC ↑
UNet [20]	10.19	66.4	9.21	76.6	11.12	56.1	10.24	66.5
AttUNet [18]	9.97	66.4	9.00	76.7	10.45	54.3	10.46	68.3
nnUNet [11]	4.60	81.9	3.64	91.9	4.06	80.97	4.91	85.35
SETR NUP [29]	13.78	63.7	14.419	69.7	11.72	54.4	15.19	66.9
SETR PUP [29]	14.01	63.8	15.245	69.6	11.76	54.9	15.023	67.0
SETR MLA [29]	13.49	63.9	15.503	69.8	10.24	55.4	14.72	66.5
TransUNet [6]	12.98	64.4	14.03	70.6	10.42	54.2	14.5	68.4
TransBTS [25]	9.65	69.6	10.03	77.9	9.97	57.4	8.95	73.5
CoTr [27]	9.70	68.3	9.20	74.6	9.45	55.7	10.45	74.8
UNETR [9]	8.82	71.1	8.27	78.9	9.35	58.5	8.85	76.1
nnFormer [30]	4.05	86.4	3.80	91.3	3.87	81.8	4.49	86.0
VT-UNet-S	3.84	85.9	4.01	90.8	2.91	81.8	4.60	85.0
VT-UNet-B	3.43	87.1	3.51	91.9	2.68	82.2	4.10	87.2

Table 1: Segmentation Results on MSD BraTS Dataset.

	Artefact	Avg. HD95 ↓	Avg. DSC ↑
nnFormer	Clean	4.05	86.4
	Motion	4.81	84.3
	Ghost	4.30	84.5
	Spike	4.63	84.9
VT-UNet	Clean	3.43	87.1
	Motion	3.87	85.8
	Ghost	3.69	86.0
	Spike	3.50	86.6

Table 2: Robustness Analysis.

VT-UNet-B	Avg. HD95 ↓	Avg. DSC ↑
w/o FPE	85.35	4.33
w/o FPE & CA	83.58	6.18

Table 3: Ablation Study.

Implementation Details. We use 484 MRI scans from MSD BraTS task [1]. Following [9,30], we divide 484 scans into 80%, 15% and 5% for training, validation and testing sets, respectively. We use PyTorch [19], with a single Nvidia A40 GPU. The weights of Swin-T [14] pre-trained on ImageNet-22K are used to initialize the model. For training, we employ AdamW optimizer with a learning rate of $1e^{-4}$ for 1000 epochs and a batch size of 4. We used rotating, adding noise, blurring and adding gamma as data augmentation techniques.

Experimental Results. Table 1 compares VT-UNet with recent transformer based approaches and SOTA CNN based methods. We introduce variants of the VT-UNet, by changing the number of embedded dimensions used for model training. Our variants are: (a) Small *VT-UNet-S* with $C = 48$ (b) Base *VT-UNet-B* with $C = 72$. We use Dice Srensen coefficient (DSC) and Hausdorff Distance (HD) as evaluation metrics, and separately compute them for three classes: (1) Enhancing Tumor (ET), (2) the Tumor Core (TC) (addition of ET, NET and NCR), and (3) the Whole Tumor (WT) (addition of ED to TC), following similar evaluation strategy as in [11,9,30]. Our quantitative results in Table 1 suggest that VT-UNet achieves best overall performance in DSC and HD. Table 4 shows qualitative segmentation results on unseen patient data. We can observe that our model can accurately segment the structure and delineates boundaries of tumor. We believe that, capturing long-range dependencies across adjacent slices plays a vital role in our model’s performance. Our empirical results in Table 3 reveal the importance of introducing Parallel CA and SA together with FPE in

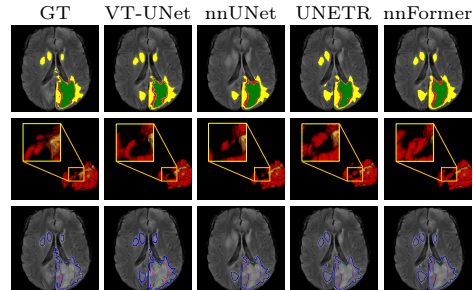


Table 4: Qualitative Segmentation Results. **Row-1:** Yellow, Green and Red represent Peritumoral Edema (ED), Enhancing Tumor (ET) and Non Enhancing Tumor (NET)/ Necrotic Tumor (NCR), respectively. **Row-2:** volumetric tumor prediction. **Row-3:** segmentation boundaries.

VT-Dec-Blks along with convex combination. We can notice that all of these components contribute towards model’s performance.

Robustness Analysis. Factors such as patient’s movement and acquisition conditions can introduce noise to MRI. Here, we investigate the robustness of VT-UNet, by synthetically introducing artefacts to MR images at inference time. These include **(1)** Motion artefacts [22]. **(2)** Ghosting artefacts [3]. **(3)** Spike artefacts (Herringbone artefact) [12]. Table 2 compares the robustness of our method with nnFormer [30]. The results suggest that VT-UNet performs more reliably in the presence of these nuisances. Our findings are consistent with existing works on RGB images, where Transformer based models have shown better robustness against occlusions [17], natural and adversarial perturbations [21,17], owing to their highly dynamic and flexible receptive field.

5 Conclusion

This paper presents a volumetric transformer network for medical image segmentation, that is computationally efficient to handle large-sized 3D volumes, and learns representations that are robust against artefacts. Our results show that the proposed model achieves consistent improvements over existing state-of-the-art methods in volumetric segmentation. We believe our work can assist better clinical diagnosis and treatment planning.

References

1. Antonelli, M., Reinke, A., Bakas, S., Farahani, K., Landman, B.A., Litjens, G., Menze, B., Ronneberger, O., Summers, R.M., van Ginneken, B., et al.: The medical segmentation decathlon. arXiv preprint arXiv:2106.05735 (2021) 8
2. Arnab, A., Deghani, M., Heigold, G., Sun, C., Lučić, M., Schmid, C.: Vivit: A video vision transformer. arXiv preprint arXiv:2103.15691 (2021) 7
3. Axel, L., Summers, R., Kressel, H., Charles, C.: Respiratory effects in two-dimensional fourier transform mr imaging. *Radiology* **160**(3), 795–801 (1986) 9
4. Cao, H., Wang, Y., Chen, J., Jiang, D., Zhang, X., Tian, Q., Wang, M.: Swin-unet: Unet-like pure transformer for medical image segmentation. arXiv preprint arXiv:2105.05537 (2021) 1, 2, 7
5. Carion, N., Massa, F., Synnaeve, G., Usunier, N., Kirillov, A., Zagoruyko, S.: End-to-end object detection with transformers. In: *European Conference on Computer Vision*. pp. 213–229. Springer (2020) 1
6. Chen, J., Lu, Y., Yu, Q., Luo, X., Adeli, E., Wang, Y., Lu, L., Yuille, A.L., Zhou, Y.: Transunet: Transformers make strong encoders for medical image segmentation. arXiv preprint arXiv:2102.04306 (2021) 1, 7, 8
7. Chen, L.C., Papandreou, G., Kokkinos, I., Murphy, K., Yuille, A.L.: Deeplab: Semantic image segmentation with deep convolutional nets, atrous convolution, and fully connected crfs. *IEEE transactions on pattern analysis and machine intelligence* **40**(4), 834–848 (2017) 5
8. Dosovitskiy, A., Beyer, L., Kolesnikov, A., Weissenborn, D., Zhai, X., Unterthiner, T., Deghani, M., Minderer, M., Heigold, G., Gelly, S., et al.: An image is worth 16x16 words: Transformers for image recognition at scale. arXiv preprint arXiv:2010.11929 (2020) 1, 7

9. Hatamizadeh, A., Tang, Y., Nath, V., Yang, D., Myronenko, A., Landman, B., Roth, H.R., Xu, D.: Unetr: Transformers for 3d medical image segmentation. In: Proceedings of the IEEE/CVF Winter Conference on Applications of Computer Vision. pp. 574–584 (2022) [2](#), [7](#), [8](#)
10. Hu, H., Zhang, Z., Xie, Z., Lin, S.: Local relation networks for image recognition. In: Proceedings of the IEEE/CVF International Conference on Computer Vision. pp. 3464–3473 (2019) [3](#)
11. Isensee, F., Maier-Hein, K.H.: nnu-net for brain tumor segmentation. In: Brain-lesion: Glioma, Multiple Sclerosis, Stroke and Traumatic Brain Injuries: 6th International Workshop, BrainLes 2020, Held in Conjunction with MICCAI 2020, Lima, Peru, October 4, 2020, Revised Selected Papers, Part II. vol. 12658, p. 118. Springer Nature (2021) [8](#)
12. Jin, K.H., Um, J.Y., Lee, D., Lee, J., Park, S.H., Ye, J.C.: Mri artifact correction using sparse+ low-rank decomposition of annihilating filter-based hankel matrix. *Magnetic resonance in medicine* **78**(1), 327–340 (2017) [9](#)
13. Khan, S., Naseer, M., Hayat, M., Zamir, S.W., Khan, F.S., Shah, M.: Transformers in vision: A survey. arXiv preprint arXiv:2101.01169 (2021) [3](#)
14. Liu, Z., Lin, Y., Cao, Y., Hu, H., Wei, Y., Zhang, Z., Lin, S., Guo, B.: Swin transformer: Hierarchical vision transformer using shifted windows. arXiv preprint arXiv:2103.14030 (2021) [2](#), [4](#), [5](#), [7](#), [8](#)
15. Liu, Z., Ning, J., Cao, Y., Wei, Y., Zhang, Z., Lin, S., Hu, H.: Video swin transformer. arXiv preprint arXiv:2106.13230 (2021) [1](#), [5](#), [7](#)
16. Milletari, F., Navab, N., Ahmadi, S.A.: V-net: Fully convolutional neural networks for volumetric medical image segmentation. In: 2016 fourth international conference on 3D vision (3DV). pp. 565–571. IEEE (2016) [5](#)
17. Naseer, M., Ranasinghe, K., Khan, S., Hayat, M., Khan, F.S., Yang, M.H.: Intriguing properties of vision transformers. arXiv preprint arXiv:2105.10497 (2021) [7](#), [9](#)
18. Oktay, O., Schlemper, J., Folgoc, L.L., Lee, M., Heinrich, M., Misawa, K., Mori, K., McDonagh, S., Hammerla, N.Y., Kainz, B., et al.: Attention u-net: Learning where to look for the pancreas. arXiv preprint arXiv:1804.03999 (2018) [5](#), [8](#)
19. Paszke, A., Gross, S., Chintala, S., Chanan, G., Yang, E., DeVito, Z., Lin, Z., Desmaison, A., Antiga, L., Lerer, A.: Automatic differentiation in pytorch (2017) [8](#)
20. Ronneberger, O., Fischer, P., Brox, T.: U-net: Convolutional networks for biomedical image segmentation. In: MICCAI. pp. 234–241. Springer (2015) [5](#), [8](#)
21. Shao, R., Shi, Z., Yi, J., Chen, P.Y., Hsieh, C.J.: On the adversarial robustness of visual transformers. arXiv preprint arXiv:2103.15670 (2021) [1](#), [7](#), [9](#)
22. Shaw, R., Sudre, C., Ourselin, S., Cardoso, M.J.: Mri k-space motion artefact augmentation: model robustness and task-specific uncertainty. In: International Conference on Medical Imaging with Deep Learning–Full Paper Track (2018) [9](#)
23. Touvron, H., Cord, M., Douze, M., Massa, F., Sablayrolles, A., Jégou, H.: Training data-efficient image transformers & distillation through attention. In: International Conference on Machine Learning. pp. 10347–10357. PMLR (2021) [7](#)
24. Vaswani, A., Shazeer, N., Parmar, N., Uszkoreit, J., Jones, L., Gomez, A.N., Kaiser, Ł., Polosukhin, I.: Attention is all you need. In: Advances in neural information processing systems. pp. 5998–6008 (2017) [2](#), [3](#), [6](#), [12](#)
25. Wang, W., Chen, C., Ding, M., Yu, H., Zha, S., Li, J.: Transbts: Multimodal brain tumor segmentation using transformer. In: International Conference on Medical Image Computing and Computer-Assisted Intervention. pp. 109–119. Springer (2021) [2](#), [7](#), [8](#)

26. Wang, Z., Liu, J.C.: Translating math formula images to latex sequences using deep neural networks with sequence-level training. *International Journal on Document Analysis and Recognition (IJDAR)* **24**(1), 63–75 (2021) [12](#)
27. Xie, Y., Zhang, J., Shen, C., Xia, Y.: Cotr: Efficiently bridging cnn and transformer for 3d medical image segmentation. arXiv preprint arXiv:2103.03024 (2021) [8](#)
28. Yuan, L., Chen, Y., Wang, T., Yu, W., Shi, Y., Jiang, Z., Tay, F.E., Feng, J., Yan, S.: Tokens-to-token vit: Training vision transformers from scratch on imagenet. arXiv preprint arXiv:2101.11986 (2021) [2](#)
29. Zheng, S., Lu, J., Zhao, H., Zhu, X., Luo, Z., Wang, Y., Fu, Y., Feng, J., Xiang, T., Torr, P.H., et al.: Rethinking semantic segmentation from a sequence-to-sequence perspective with transformers. In: *Proceedings of the IEEE/CVF Conference on Computer Vision and Pattern Recognition*. pp. 6881–6890 (2021) [7](#), [8](#)
30. Zhou, H.Y., Guo, J., Zhang, Y., Yu, L., Wang, L., Yu, Y.: nnformer: Interleaved transformer for volumetric segmentation. arXiv preprint arXiv:2109.03201 (2021) [2](#), [7](#), [8](#), [9](#)
31. Zhou, Z., Siddiquee, M.M.R., Tajbakhsh, N., Liang, J.: Unet++: A nested u-net architecture for medical image segmentation. In: *Deep Learning in Medical Image Analysis and Multimodal Learning for Clinical Decision Support*, pp. 3–11. Springer (2018) [5](#)

6 Supplementary Material

Preliminaries Here we provide a brief description about the SA. In SA, we are interested in generating a new sequence of tokens, $\{\mathbf{z}_1, \mathbf{z}_2, \dots, \mathbf{z}_\tau\}$, from \mathbb{X} to better represent our signal according to the objective of learning. In doing so, we can assume that \mathbf{x}_i s span a subset of \mathbb{R}^C and define \mathbf{z}_i as a point in that span, *i.e.* $\mathbf{z}_i = \sum_j a_{ij} \mathbf{x}_j$, where a_{ij} s are combination values defined by \mathbf{x}_i and \mathbf{x}_j . A possible choice for a_{ij} is based on the similarity of \mathbf{x}_i and \mathbf{x}_j , which algebraically is proportional to $\langle \mathbf{x}_i, \mathbf{x}_j \rangle$. Such a choice enables us to define the token \mathbf{z}_i by attending to important parts of the input sequence according to the objective in hand, hence the name attention. We can take a further step and put a constraint on our design by enforcing the generated tokens to lie inside the convex hull defined by \mathbf{x}_i s. In that case, we will have $\mathbf{z}_i = \sum_j a_{ij} \mathbf{x}_j, a_{ij} \geq 0, \sum_j a_{ij} = 1$. The convex hull formulation endows nice properties, one being that the resulting tokens cannot grow boundlessly, given the fact that the input is assumed to be a natural signal. The SA operation is built upon the above idea with some modifications. Firstly, we assume that tokens, in their original form, might not be optimal for defining the span. Therefore, in SA we define the span by learning a linear mapping from the input tokens. This we can show with $\mathbb{R}^{\tau \times C_v} \ni \mathbf{V} = \mathbf{X} \mathbf{W}_V$, where we stack tokens \mathbf{x}_i s into the rows of \mathbf{X} (*i.e.*, $\mathbf{X} = [\mathbf{x}_1 | \mathbf{x}_2 | \dots | \mathbf{x}_\tau]^\top$). Then we turn our attention to a_{ij} and define it by learning two linear mappings, following a similar argument. In particular, first we define a set of keys from \mathbf{x}_i as $\mathbb{R}^{\tau \times C_k} \ni \mathbf{K} = \mathbf{X} \mathbf{W}_K$. To generate a_{ij} , we measure the similarity of a transformed version of \mathbf{x}_i , which we call the query $\mathbf{q}_i = \mathbf{W}_Q^\top \mathbf{x}_i$, with respect to the keys \mathbf{k}_j that are represented by the rows of \mathbf{K} . That is, $a_{ij} \propto \langle \mathbf{q}_i, \mathbf{k}_j \rangle$. Put everything into a matrix form and opt for a softmax function to achieve the constraints $a_{ij} \geq 0$ and $\sum_j a_{ij} = 1$, we arrive at Eq (1).

Breaking Symmetry Cont. The linear patch-projection flattens the features, thereby failing to fully encapsulate object-aware representations (e.g., spatial information) that are critical for anatomical pixel-wise segmentation. As shown in Fig. 2(e), combining two sets of tokens may results in loss of fluency. Therefore, in order to preserve features among continuous slices, we supplement the 3D Fourier Feature Positional Encoding (FPE) for the tokens generated from MSA module by adapting sine and cosine functions with different frequencies [24], which provides unique encoding for each input token. Following work by Wang *et al.* [26], we used the extended version of 2D positional encoding for 3D. Therefore, we call this as a 3D FPE or in other words a 3D positional encoding with a sinusoidal input mapping for VT-Dec-Blks. After applying 3D FPE to tokens, we pass it through a LN and MLP layer. Our empirical evaluations confirm that adding a Fourier feature positional bias can improve the poor conditioning of the feature representation.

Loss Function. To train VT-UNet, we jointly minimize the Dice Loss together with Cross Entropy loss (computed in a voxel-wise manner).